JOURNAL OF PROPULSION AND POWER
Vol. 23, No. 6, November–December 2007

Measurements of Current Distribution on a Two-Grid Ion-Extraction-System Gridlet

Yukio Hayakawa*
Japan Aerospace Exploration Agency, Chofu, Tokyo 182-8522, Japan

DOI: 10.2514/1.28432

Numerical models of ion extraction used in the design of ion thrusters need to be validated by comparison with experimental data; in particular, the magnitudes of ion-impingement currents as functions of screen and discharge voltages should be quantified. This paper provides measurements which may be used to test numerical models of ion extraction using two multiple-hole grids. A grid set, in which an isolated gridlet was embedded in an accelerator grid, was built to measure ion-impingement current distribution. The gridlet was composed of barrel and downstream electrodes, electrically isolated from each other and the rest of the accelerator grid. The obtained measurements of ion-impingement currents on the electrodes can be directly compared with numerical predictions. The barrel-electrode current has been found not to be proportional to the downstream-electrode current, a fact which cannot be shown by measurement of the total accelerator-grid current. This current was also observed to significantly depend not only on screen voltage but also on discharge voltage, whereas the downstream-electrode current was found to be insensitive to both voltages. The total accelerator-grid current was influenced by both of these.

Nomenclature

J_a	=	accelerator-grid current, $J_{g0} + J_{a6}$
J_{a6}	=	accelerator-grid current excluding J_{g0}
J_b	=	beam current
J_{ba}	=	barrel-electrode current
J_{b0}	=	beamlet current
J_{ds}	=	downstream-electrode current
J_{g0}	=	center-gridlet current, $J_{\mathrm{ba}} + J_{\mathrm{ds}}$
J_n	=	neutralizer's electron-emission current
J_{sp}	=	beam-separator current
J_t	=	tank current
l_g	=	screen-to-accelerator grid separation
N_n	=	neutral-atom number density
t_a	=	accelerator-grid thickness
t_s	=	screen-grid thickness
V_a	=	accelerator-grid voltage
V_d	=	discharge voltage
V_s	=	screen voltage
σ_{ce}	=	charge-exchange cross section

I. Introduction

ION thrusters are devices that propel spacecraft by using electrical energy to produce high-speed, highly directional ions. Because the speed of the ions is much greater than the exhaust velocities of conventional chemical thrusters, efficiency is greater and significant savings on propellant mass can be made. The ion-extraction system is an important part of an ion thruster, and the accelerator grid is a critical component of this. The accelerator grid is inevitably struck by particles and eroded, and this erosion is a factor that can limit the life of the ion thruster. Predicting or confirming the life of the accelerator grid is therefore one of the most important issues in ion thruster development. Determining this solely by experiment is possible, but inefficient. Alternatively, computer simulations can be powerful tools, but an important issue is qualifying the numerical models on which they are based.

Numerical models are evaluated by comparing the results of calculations with reference experimental measurements. However, a question is which quantities (or qualities) should be compared. For example, erosion-formed geometry is characterized by several variables: pit depth, width, area, and volume. Such comparisons usually require significant time and cost to obtain both eroded reference samples and calculations. However, even if these are found to be in good agreement, the numerical models are not necessarily sufficiently qualified. If the models are to be reliable, internal variables such as grid current distributions must also agree. Comparison of geometrical quantities should thus be performed in the final stage of model qualification, and other quantities must be sought which are simpler and quicker to validate.

Ion current distribution offers an alternative which can make model qualification simpler, quicker, and more fundamental. Because many 3-D numerical models deal with a single gridlet using periodic boundary conditions to reduce computation load [1–9], contours would seem a convenient reference quantity. In previous experiments by our group, ion beamlet contours downstream of seven-hole grids have been measured and published as reference data for validating numerical calculations [10,11]. However, the comparison of contours may not be as simple as expected, and beam ions, which mainly comprise the contours, are not the only particles that erode the grid. As a result, contours have not been used as a reference quantity hitherto.

In this experiment, the center barrel of a seven-hole accelerator grid was replaced by an isolated barrel electrode, so that the ion-impingement current on it could be measured [12]. The obtained current data may be the first set of measurements that can be easily compared with numerical models. Comparing currents is quick, simple, and fundamental, and both experiments and simulations do not require either long periods of time or high costs to perform.

In this study, two electrodes, a barrel, and a downstream electrode, were embedded in a seven-hole accelerator grid and together formed the center gridlet. The number of test cases was increased from the previous experiments [12] due to the addition of two operating parameters: screen and discharge voltage.

II. Apparatus and Procedure

A cutaway drawing of the ion thruster used in this study is shown in Fig. 1. This consisted of a discharge chamber, originally used in a 14-cm xenon ion thruster, equipped with both screen and accelerator

Presented as Paper 5003 at the 42nd AIAA/ASME/SAE/ASEE Joint Propulsion Conference & Exhibit, Sacramento, California, 9–12 July 2006; received 20 October 2006; revision received 19 July 2007; accepted for publication 19 July 2007.

*Senior Research Engineer, Spacecraft Propulsion Engineering Group, 7-44-1 Jindaijihigashi-machi. Senior Member.

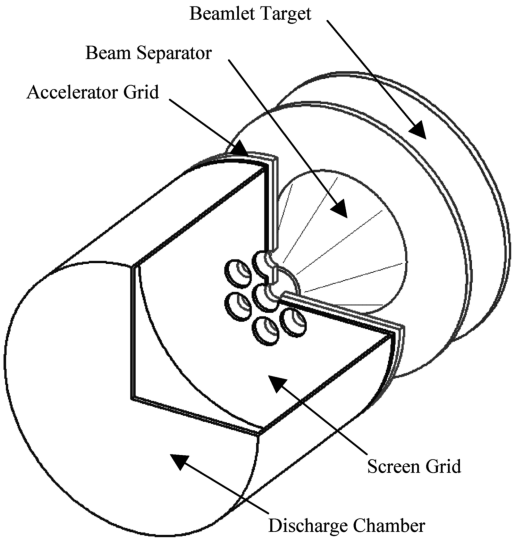

Fig. 1 Thruster components.

grids with a centerline hole surrounded by six holes. A baffle was placed in front of a hollow cathode to facilitate stable discharge at very low discharge currents. A conical beam separator, with a 30-deg half-angle with its apex cut off, was located downstream of the accelerator grid and intercepted all beamlets except the one at the thruster centerline. A flat beamlet target downstream of the separator was used to measure the center beamlet current directly. The grids, beam separator, and beamlet target were fabricated from stainless steel. Table 1 shows the dimensions of the ion-extraction system. The accelerator grid was thicker by 0.5 mm than that in the previous experiment [12].

The separator and beamlet target were only installed in the thruster when measuring the center beamlet current, because material sputtered from these was deposited on the accelerator grid and quickly destroyed the isolation between the gridlet electrodes and the surrounding grid. Gridlet current measurement was not performed simultaneously with beamlet current measurement. This particular measurement related the center beamlet current to the whole beam current. Though the center beamlet current could not be obtained directly without the separator or target, it could be accurately calculated from the beam current.

Figure 2 shows the structure of the accelerator grid, the center gridlet of which was composed of a barrel electrode and a downstream electrode. Each electrode was electrically isolated from the other and the accelerator base. The gaps between them were filled with alumina-ceramic glue. The upstream surface of the gridlet belonged to the barrel electrode because no sign of erosion has ever been found except along the edge of an aperture of real accelerator grids, and therefore no independent electrode was required. This grid was composed of three layers, and two insulated wires individually penetrated the middle layer. Each electrode was in contact with a wire, the other end of which was connected to an ammeter outside the vacuum tank. Figure 3 shows a close-up photograph of the accelerator grid, and several voids are seen in the ceramic glue. The resistances between the electrodes and grid were several megohms or greater, and leakage currents were thus negligible.

An electrical schematic of the thruster and its diagnostic equipment is shown in Fig. 4. Several currents, including the beam

Table 1 Dimensions of the ion-extraction system

Screen-hole diameter	10 mm
Accelerator-hole diameter	8 mm
Hole center-to-center distance	11 mm
t_s	1.5 mm
t_a	3.0 mm
l_g	3.25 (3.75) mm

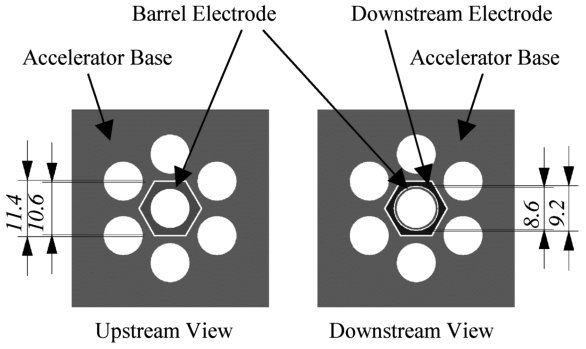

Fig. 2 Structure of accelerator grid.

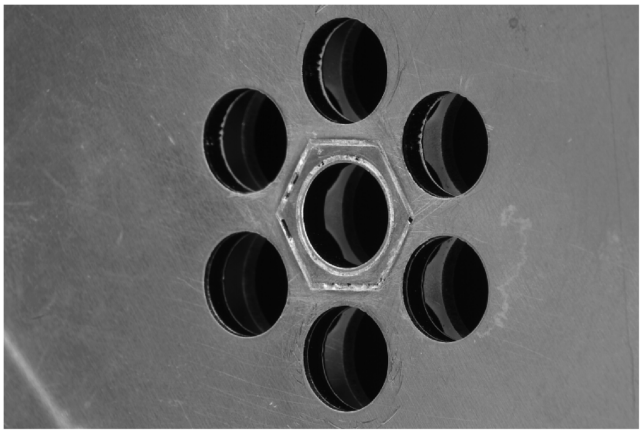

Fig. 3 Close-up photograph of the accelerator grid.

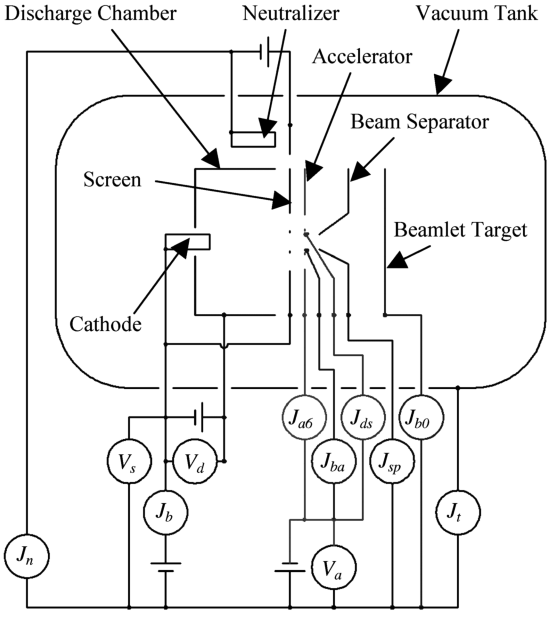

Fig. 4 Electrical schematic.

current, were measured with digital multimeters isolated from the ground. The beam separator, beamlet target, vacuum tank, and neutralizer were each grounded through an ammeter. Xenon was used as propellant. The fixed operating parameters employed are shown in Table 2. The beam current was altered by varying the discharge current, and the cathode-heater current was regulated to maintain a certain discharge voltage. Although the electron temperature had not been measured in this series of experiments, a former experiment suggests that a probable electron temperature range is less than 4 eV [13].

Table 2 Fixed operating parameters

V_a	−200 V
Main-keeper current	0.5 A
Neutralizer-keeper current	0.8 A
Discharge-chamber flow rate	38(40) ± 13 mA eq.
Neutralizer flow rate	21(24) ± 13 mA eq.

Table 3 Estimation of uncertainty

Item	Uncertainty (bias)
Beamlet current	0.6 μA
Barrel-electrode current	0.21 μA
Downstream-electrode current	0.21 μA

Sanwa PC5000 digital multimeters were used to measure beam, barrel-electrode, and downstream-electrode currents. An estimation of uncertainty is summarized in Table 3. Bias uncertainty is derived from the accuracies of the digital multimeters used and the uncertainty in the beamlet current was one-seventh of that in the beam current. The adequacy of "one-seventh" is stated in the next paragraph. Precision uncertainty is neglected because readings were made after the digits settled.

III. Experimental Results

Figure 5 shows plots of a center beamlet current against a beam current. The center beamlet current was directly proportional to the beam current (close to one-seventh: 0.1429) so that it could be calculated from it directly. A leakage current superposed on the beam current was not negligible because the voltages applied were high and the measured currents low, and so an amount equivalent to the leakage current was subtracted from each beam current measurement.

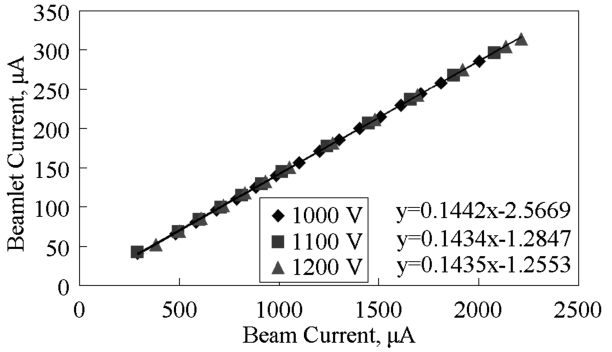

Fig. 5 Relationship between beamlet and beam currents (V_s = 1000–1200 V, V_d = 33 V).

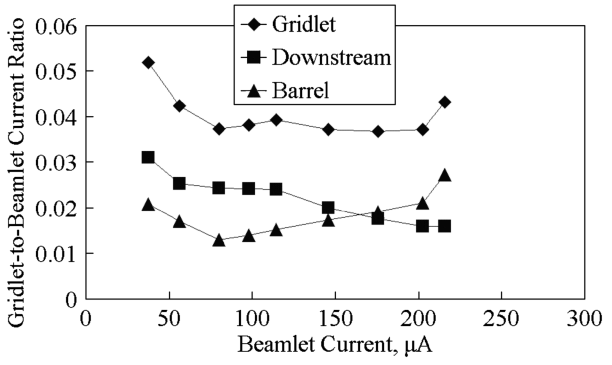

Fig. 6 Gridlet-to-beamlet current ratio (V_s = 1000 V, V_d = 33 V).

Figure 6 shows a plot of gridlet- (barrel and downstream electrodes) to-beamlet current ratio at a discharge voltage of 33 V. The plot has a flat bottom with steep slopes at both ends and is very familiar in appearance. The gridlet-to-beamlet current ratio has two components, a barrel-to-beamlet current ratio and a downstream-to-beamlet current ratio, plotted also in Fig. 6, and these have different appearances. The barrel-to-beamlet current ratio forms an upward-sloping curve while the gridlet-to-beamlet current ratio has a flat bottom. On the other hand, the downstream-to-beamlet current ratio forms a downward-sloping curve in the same range. These combine to yield the flat bottom observed in the gridlet-to-beamlet current ratio plot.

When comparing numerical model results with experimental data, currents are preferable to current ratios because the former are simpler and the latter are strongly affected by beamlet current errors. The current measurements are shown in Figs. 7–14. Bumps appear on the plots in Fig. 9: $V_s = 1000$ V, $J_{b0} \approx 90$ μA; $V_s = 1100$ V, $J_{b0} \approx 105$ μA, and Fig. 13 shows their reproducibility. The three plots in Fig. 13 were obtained on different days, and the ion-extraction system was reassembled between the measurement of

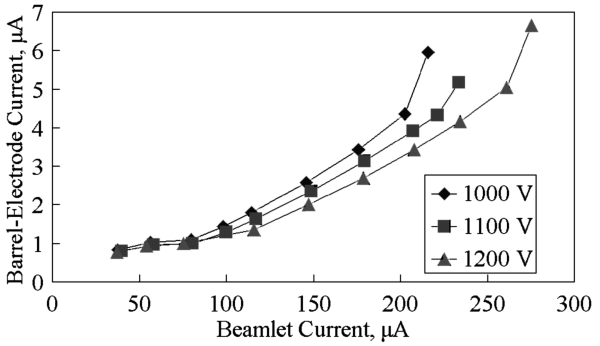

Fig. 7 Barrel-electrode current (V_s = 1000–1200 V, V_d = 33 V).

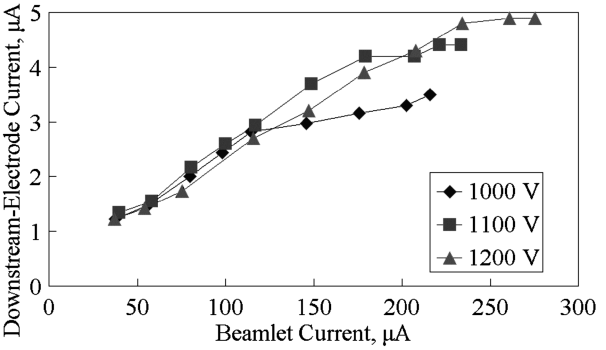

Fig. 8 Downstream-electrode current (V_s = 1000–1200 V, V_d = 33 V).

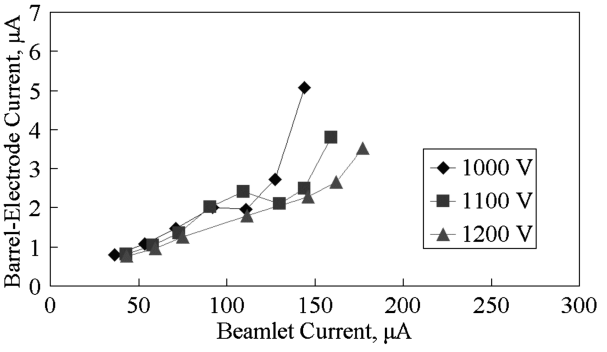

Fig. 9 Barrel-electrode current (V_s = 1000–1200 V, V_d = 30 V).

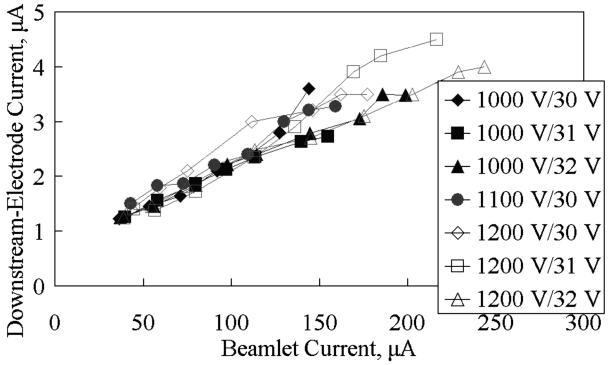

Fig. 10 Downstream-electrode current (V_s = 1000–1200 V, V_d = 30–32 V).

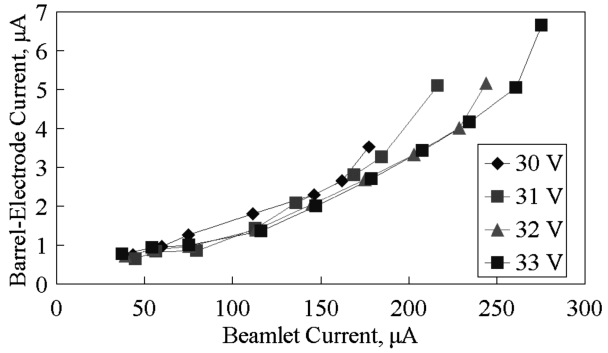

Fig. 11 Barrel-electrode current (V_s = 1200 V, V_d = 30–33 V).

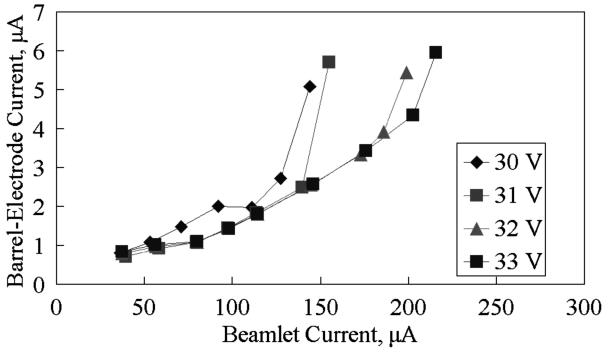

Fig. 12 Barrel-electrode current (V_s = 1000 V, V_d = 30–33 V).

plot 1 and the others. As a result of the bump, the current ratio plots corresponding to the test runs in Fig. 13 do not form flat-bottomed profiles like Fig. 6. Figure 14 shows plots under the conditions that the grid separation was 3.75 mm, the discharge-chamber flow rate was 40 ± 13 mA eq. (equivalent), and the neutralizer flow rate was 24 ± 13 mAeq.. The tank pressure for Figs. 9–13 was 5.3×10^{-4} Pa, and that for Fig. 14 was 5.6×10^{-4} Pa (both not corrected for Xe). The no-load pressure for all figures was about 3×10^{-5} Pa.

IV. Discussion

In explaining the formation of the flat-bottomed profile shown in Fig. 6, the results support a supposition that beam-ion impingement is rare and charge-exchanged-ion impingement is almost exclusive, as expressed by the formula

$$J_{\mathrm{ba}} \propto N_n \sigma_{\mathrm{ce}} (t_s + l_g + t_a) J_{b0} \tag{1}$$

In other words, the barrel-electrode current is proportional to the beamlet current as long as beam-ion impingement is rare. To explain

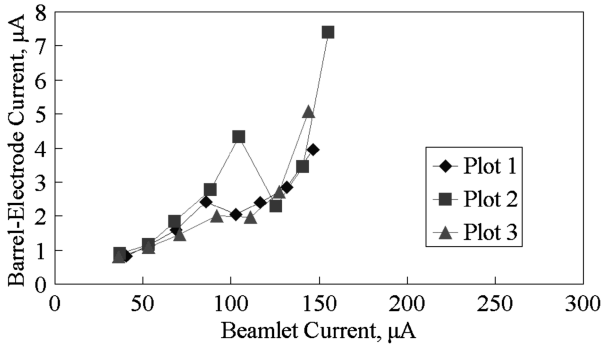

Fig. 13 Reproducibility of bumps in the barrel-electrode current (V_s = 1000 V, V_d = 30 V).

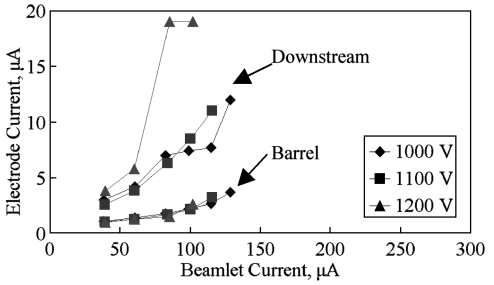

Fig. 14 Barrel- and downstream-electrode current (l_g = 3.75 mm, V_s = 1000–1200 V, V_d = 33 V).

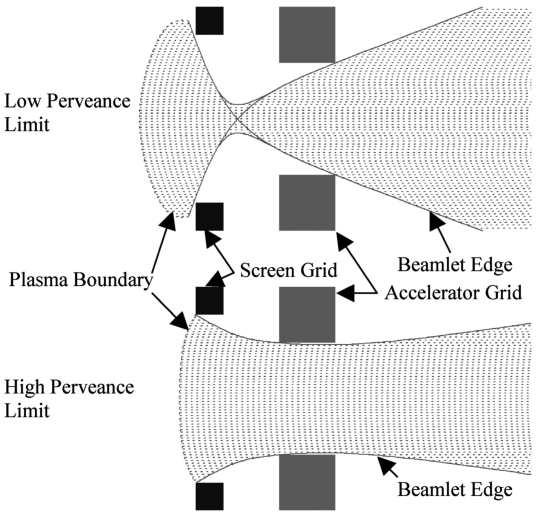

Fig. 15 Critical beamlet current conditions.

the steep slopes at both ends of the flat bottom, it was supposed that beam ions could impinge on the grid because the divergence of the beamlet can be quite large at the left end of the flat bottom, and that they could do the same at the right end of the flat bottom because the outside diameter of the beamlet can be large in this region (see Fig. 15). However, the first half of this hypothesis was proved not always true because no ion trajectories hit the accelerator grid in the simulation in a certain case [6]. The best guess at this time is that elastic scatter changes the ion trajectories.

In explaining the appearances of the plots in Fig. 6, the previous paper [12] introduced a hypothesis that if the beamlet current is lower than a critical value, the ion trajectories concentrate (see Fig. 16). This phenomenon can be reproduced in numerical simulations. The number density of charge-exchanged ions can be very high where the ion trajectories concentrate, and reducing the beamlet current below the critical value moves the position of concentration upstream. If

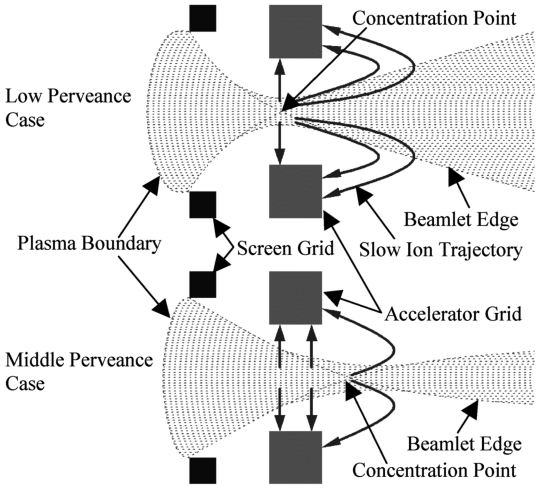

Fig. 16 Charge-exchanged ion flow (hypothesis).

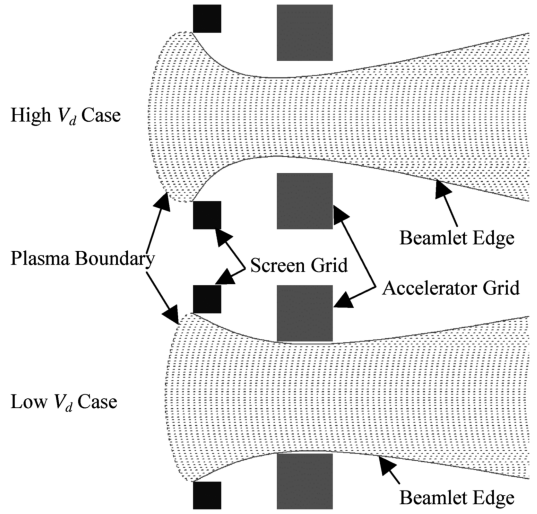

Fig. 17 Effects of discharge voltage on plasma boundary and beamlet diameter (hypothesis).

ion–ion collisions were ignored, some of the charge-exchanged ions would have their own trajectories to the accelerator grid that would be determined by both electric field and their origins. Ion–ion collisions make the beam ions push charge-exchanged ions downstream, and some of the charge-exchanged ions, which would otherwise have impinged on the barrel if collisions did not occur, consequently impinge on the downstream face of the grid.

Figures 7 and 9 suggest the following two points, Fig. 7 more strongly so than Fig. 9.

1) The increase in ion speed reduces the barrel-electrode current. This coincides with the fact that an increase in ion-neutral relative speed decreases the charge-exchange cross section [14,15].

2) The increase in screen voltage increases the critical beamlet current, where the inclination of each plot abruptly rises, and this reduces the outside diameter of a beamlet.

Both Figs. 11 and 12 suggest that an increase in discharge voltage decreases the diameter of the beamlet, and has no effect on the quantities of the barrel-electrode current unless beam ions impinge on the barrel electrode. This leads to the following hypothesis and fact:

Hypothesis: The geometry of the plasma boundary depends on the discharge voltage. An increase in discharge voltage deepens the concavity of the boundary and accordingly makes the beamlet slenderer (see Fig. 17).

Fact: A slight difference in discharge voltage changes the ion speed a little so that the charge-exchange cross section also changes slightly.

This hypothesis suggests that raising the discharge voltage is a way to increase ion beam current density, although it may shorten the life of the thruster. Martin and Latham [16] reported on an ion thruster with a grid diameter of only 10 cm that has produced an extraordinarily high thrust of 71 mN. The very high discharge voltage (originally described as "anode voltage") of 54 V may have made this possible.

Although the barrel-electrode current was usually very stable except near both limits, the downstream-electrode current was usually unstable when the beamlet current was approximately over 100 μA. This instability resulted from ions from when the neutralizer and the current depended on the neutralizer condition at the measurement. In each of Figs. 8 and 10, no apparent differences among the downstream-electrode current plots can be found over the uncertainty due to the instability, which means that neither the screen nor the discharge voltages affect the current. However, this current may depend on the screen voltage because an increase in ion speed decreases the charge-exchange cross section. The effect of the discharge voltage on the charge-exchange cross section can be neglected as it does not change the ion speed much. The net result is that both discharge voltage and screen voltage have slight influences on the downstream-electrode current.

The bumps that appear on certain plots have yet to be explained. It seems difficult to find the mechanism without making special assumptions. A possibility is that something peculiar to this thruster, such as discharge plasma nonuniformity, occurs.

An increase in grid separation narrows the range of beamlet currents at which the ion beamlet can pass through the accelerator hole without impingement. Though the relationship between screen voltage and critical beamlet current in Fig. 14 seems contrary to that in Fig. 7, the characteristics in Fig. 14 are too weak to make any claims. The downstream-electrode current seems extraordinarily high, and this may be caused by beam ions directly impinging on the wire through an insufficiency of insulator glue or some other anomaly.

Because the barrel electrode occupies part of the downstream surface of the grid, the measured barrel-electrode current might have some characteristics of both the barrel-face and downstream-face currents. Because the downstream-electrode current was unaffected by either screen or discharge voltage, the measured trend in the barrel-electrode current might be weak compared to the trend in the barrel-face current.

A. Error Factors

This series of experiments included the following error factors:

1) Noise and instability: In general, the barrel-electrode current exhibited much less fluctuation than the downstream-electrode current, and consequently is more suitable as a reference for comparison with numerical model calculations. In addition, the latter was more affected by neutralizer activity than the former, and its electron-emission current, in fact, had both fluctuations and jumps. The barrel-electrode current generally was settled down to the order of 0.01 μA unless the beamlet impinged the electrode. On the other hand, the downstream-electrode current was usually settled down to the order of 0.1 μA over the region.

2) Leakage current: The wiring, which was held at the accelerator-grid voltage, was partially exposed to open space and so ions could be attracted by it. However, the leakage current is thought to be very small because the exposed wiring was located far from the ion beamlets.

3) Isolation gaps: There may be influences due to the gaps, which would not exist in a real thruster. However, these influences can be estimated in the process of comparison with calculations, as discussed below.

4) Configuration errors: The dimensional tolerances of components, changes in component alignment during assembly, and the effects of erosion result in errors. Thermal deformation is also included in this category. The data obtained were usually different before and after reassembly. However, no two measurements in each graph were separated by reassembly except those in Fig. 13, and

hence the influences of these errors on the characteristics of the plots can be ignored.

B. Comparison with Calculations

Because of the errors that inevitably accompany experiments, the obtained measurements are not perfect references for numerical models. In addition, the neutral-atom density distribution near the grids is not measurable, and so must be guessed. Even though comparing the magnitudes of currents between experimental and simulation data is meaningful, it is not sufficient. Identifying the qualitative characteristics of the experimental plots and verifying that these characteristics also appear in the numerical calculations is also important.

Before remarking on the characteristics individually, the following proposals are made regarding the treatment of the isolation gaps on the accelerator grid:

1) Treating them as insulators: This choice most closely models the gaps and would therefore yield the best results, but makes the simulations more difficult to implement.

2) Putting a virtual border in the middle of each gap, and assuming the gap as both a conductor and a part of the grid: The current due to ions which would impinge on the gap if the gap were electrically a part of the grid does not necessarily separate into halves.

3) Putting virtual borders on both edges of each gap, assuming the gap as both a conductor and a part of the grid, and assuming the current to where the gap is supposed to be as an error current for each electrode current: The error bars in this method will be the tallest among these three methods, but numerical models will not be made complicated, and the error is treated properly.

C. Statistical Analysis

The barrel-electrode and downstream-electrode currents are expressed by using a multiple regression analysis method, as follows;

$$J_{\mathrm{ba}} = 6.46 - 0.00236V_s - 0.130V_d + 0.00202J_{b0} \tag{2}$$

$$J_{\mathrm{ds}} = 2.28 + 0.00135V_s + 0.0435V_d + 0.00181J_{b0} \tag{3}$$

Here the data beyond the perveance limits have been excluded before analyzing. The coefficient of determination adjusted for the degrees of freedom is 0.854 for both equations and they are significant at the 1% level. Every multiple regression coefficient in Eq. (2) is significant at the 1% level. On the other hand, in Eq. (3), the coefficient for the screen voltage is significant at the 5% level; that for the discharge voltage is not significant at the 5% level; that for the beamlet current is significant at the 1% level.

Several facts have been found in the series of experiments as follows:

1) The greatest beamlet current at which beam-ion impingement on the grid does not occur is higher at a discharge voltage of 33 V than 30 V.

2) The greatest beamlet current at which beam-ion impingement on the grid does not occur is higher at a screen voltage of 1200 V than 1000 V.

3) An increase in the screen voltage decreases the barrel-electrode current, and this is apparent at a discharge voltage of 33 V.

4) There is a bump on the current plots at a screen voltage of 1000 V and a discharge voltage of 30 V.

5) No apparent differences are found between downstream-electrode plots at different screen and discharge voltages.

6) Increasing grid separation to 3.75 mm reduces the beamlet current operation range by half compared to a separation of 3.25 mm.

V. Conclusions

This paper presents measurements of ion-impingement currents on the electrodes which can be used as reference data for validating numerical models. A barrel-electrode current was observed to be significantly dependent not only on screen voltage but also on discharge voltage, while a downstream-electrode current was found to be insensitive to both voltages. Probable sources of measurement errors are mentioned, and comments are made on points to be considered in comparing the measurements and numerical calculations.

References

[1] Hayakawa, Y., "Three-Dimensional Numerical Model of Ion Optics System," *Journal of Propulsion and Power*, Vol. 8, No. 1, 1992, pp. 110–117.

[2] Peng, X., Keefer, D., and Ruyten, W., "Plasma Particle Simulation of Electrostatic Ion Thrusters," *Journal of Propulsion and Power*, Vol. 8, No. 2, 1992, pp. 361–366.

[3] Nakano, M., and Arakawa, Y., "Development of an Efficient Three-Dimensional Optics Code," IEPC Paper 97-015, Aug. 1997.

[4] Nakayama, Y., and Wilbur, P. J., "Numerical Simulation of Ion Beam Optics for Multiple-Grid Systems," *Journal of Propulsion and Power*, Vol. 19, No. 4, 2003, pp. 607–613.

[5] Wang, J., Polk, J., Brophy, J., and Katz, I., "Three-Dimensional Particle Simulations of Ion Optics Plasma Flow and Grid Erosion," *Journal of Propulsion and Power*, Vol. 19, No. 6, 2003, pp. 1192–1199.

[6] Okawa, Y., Hayakawa, Y., and Kitamura, S., "Three-Dimensional Divergence Characteristics of Ion Beamlets in an Ion Thruster," AIAA Paper 2004-3785, July 2004.

[7] Williams, G. J., Jr., Sovey, J. S., and Haarg, T. W., "Characterization of High-Specific Impulse, High-Power Ion Optics," AIAA Paper 2004-3630, July 2004.

[8] Malone, S. P., and Soulas, G. C., "Computational Ion Optics Design Evaluations," AIAA Paper 2004-3784, July 2004.

[9] Farnell, C. C., "Numerical Simulation of HiPEP Ion Optics," AIAA Paper 2004-3818, July 2004.

[10] Hayakawa, Y., Kitamura, S., and Miyazaki, K., "Beamlet Profiles from Multiple-Hole Ion-Extraction Systems," *Journal of Propulsion and Power*, Vol. 14, No. 4, 1998, pp. 568–574.

[11] Hayakawa, Y., and Kitamura, S., "Ion Beamlet Divergence Characteristics of Two-Grid Multiple-Hole Ion-Accelerator Systems," *Journal of Propulsion and Power*, Vol. 15, No. 3, 1999, pp. 377–382.

[12] Hayakawa, Y., Okawa, Y., and Kitamura, S., "Experiments to Find the Origins of Highly Diverged Ions," AIAA Paper 2005-3884, July 2005.

[13] Hayakawa, Y., Nakamura, Y., Kitamura, S., and Miyazaki, K., "The Experimental Investigation on 12 cm Ring Cusp Ion Thruster," *International Symposium on Space Technology and Science*, Vol. 1, 1986, pp. 97–102.

[14] Rapp, D., and Francis, W. E., "Charge Exchange Between Gaseous Ions and Atoms," *Journal of Chemical Physics*, Vol. 37, No. 11, 1962, pp. 2631–2645.
doi:10.1063/1.1733066

[15] Miller, J. S., Pullins, S. H., Levandier, D. J., Chiu, Y., and Dressler, R. A., "Xenon Charge Exchange Cross Sections for Electrostatic Thruster Models," *Journal of Applied Physics*, Vol. 91, No. 3, 2002, pp. 984–991.
doi:10.1063/1.1426246

[16] Martin, A. R., and Latham, P. M., "High Thrust Operation of the UK-10 Rare Gas Ion Thruster (T4A)," IEPC Paper 88-062, Oct. 1988.

A. Gallimore
Associate Editor